

A New Constitutive Strain Dependent Garofalo Equation to Describe the High- Temperature Processing of Materials. Application to the AZ31 Magnesium Alloy

I. RIEIRO, V. GUTIÉRREZ, J. CASTELLANOS, M. CARSI, M.T. LARREA, and O.A. RUANO

I. Rieiro, Professor, V. Gutiérrez, J. Castellanos, PhD Students, are with Dpto. Matemáticas, Universidad de Castilla-La Mancha, Avda. Carlos III s/n, 45071 Toledo, Spain. M. Carsi, M.T. Larrea, Senior Researchers, and O.A. Ruano, Professor, are with Dpto. Metalúrgica Física, Centro Nacional de Investigaciones Metalúrgicas, CENIM, CSIC, Avda. Gregorio del Amo 8, 28040 Madrid, Spain. Contact e-mail: ruano@cenim.csic.es.

* Corresponding author. Tel.: +34 915538900; Fax: +34 915347425

E-mail address: ruano@cenim.csic.es

Keywords: Magnesium alloy; Deformation and fracture; Torsion tests; Garofalo equation; Numerical methods; Constitutive equations

ABSTRACT

A new strain dependent equation derived from that of Garofalo is developed in this work. This equation describes mathematically the deformation behavior of materials as a function of strain, strain rate and temperature and is valid over a wide range of strain with good statistical accuracy. An explicit expression $\sigma(\varepsilon) = f(\varepsilon, T, \dot{\varepsilon})$ is introduced that reproduces stress-strain curves. Statistical tools for determining the validity of the equation have been applied. Predictions from this expression were compared with torsion data obtained in AZ31 magnesium alloy that was deformed at various

temperatures and strain rates. Analysis of the strain dependence of the Garofalo parameters allowed us to establish a steady state at strains of about 0.6. It also allows drawing conclusions about the microstructural changes that occur during deformation of the alloy. In addition, the characteristic points in the evolution with strain of the parameters of the equation are related to the most significant values that characterize the microstructural processes occurring during deformation of the AZ31 alloy. The observed decrease of Q and n as a function of strain is attributed first to a softening process due to dynamic recrystallization and grain size refinement and finally to flow localization. The predicted values obtained with the new constitutive equation and the experimental values for the AZ31 alloy are in good agreement with an average relative error of about 6.5 %.

I. INTRODUCTION

The Garofalo equation is a general form of the power law equation describing slip creep controlled by dislocation climb and therefore by diffusion processes. This generalization allows the equation to be applied over a large range of stresses or strain rates.^[1-3] It can be considered a state equation but only at the steady state region of stress-strain curves that are obtained from experimental data. This equation is also used at the peak stress since the condition of stress change with strain equals zero. However, the Garofalo equation is not well defined as a constitutive equation because it is not strain dependent.

An important goal of a constitutive equation is to describe various microstructural processes, through its parameters, involved in deformation as dynamic recovery or dynamic recrystallization, DRX, that may lead to the steady state and finally to flow localization and rupture of the material.^[1,4-6]

The Garofalo equation is one of the various algebraic equations used for analyzing the stress-strain curves.^[7,9] At steady state this equation is usually expressed as:

$$\dot{\epsilon} = A \cdot e^{-\frac{Q}{RT}} \cdot (\sinh(\alpha \cdot \sigma))^n \quad (1)$$

The variables are $\{\dot{\epsilon}, T, \sigma\}$, strain rate, temperature and stress, and the characterized parameters, named Garofalo parameters, A , Q , n and α , have been widely analyzed.^[10-12] Originally this was a phenomenological equation but numerous physical models justify the Garofalo equation to describe various deformation mechanisms at steady state.^[13-15]

Constitutive equations should mathematically describe the deformation behavior of materials as a function of the strain, strain rate and temperature. Therefore, the construction of constitutive equations is highly complex, and frequently the valid strain range of application is very short.^[16] However, it is important to develop this type of equations for practical reasons, related to simulations for industrial applications. Therefore, it is highly interesting to make this equation a function of strain where the solutions obtained at the peak and at the steady state should be used as control conditions.

In the last decades, several investigations have been conducted to obtain strain dependent equations to reproduce and to predict plastic flow of materials.^[17] This has been done from very different approximations and with different mathematical methods. One approximation is to calculate the Garofalo parameters at various strains. This is conducted by decomposing the dependence of the above mentioned parameters in different linearized factors that are determined by means of linear regressions. The procedure is carried out in successive stages of linear regressions by using logarithmic transformations. It is difficult by this procedure to control the cumulative errors among stages. This limits the capacity for discriminating and characterizing the controlling mechanism from these parameters. However, it is useful to reproduce the stress-strain curves.

Another approximation is to modelize the constitutive equation as a function of various $\alpha\sigma$ intervals.^[18,19] One of these intervals corresponds to the Garofalo equation and the other to the power law equation, σ^n . The main problem is the determination of the stress exponent which may lead to large errors. Other parameters, such as the activation energy, depend on the election of the n value. Therefore, the errors are accumulated from strain to strain. Mathematically, an optimization in the R^4 space is reduced to four optimizations in R^1 space.

A further approximation is to unify different partial laws at various strain intervals for the flow behavior of the material assuming one main creep mechanism for each law. These intervals are based on experimental observations.^[20,21] The main laws used correspond to Avrami and Voce, and the Garofalo equation is only used to supply some of the necessary parameters.^[22,23]

Another approximation for the construction of the constitutive equation extended for a large range of strains is based on dimensional analysis of various variables that are of physical significance such as the stacking fault energy, grain size, dislocation density, etc.^[24] This model needs a large amount of microstructural data and works with a large amount of variables. A further approach in this line is to use an equation that contains two factors, one derived from Garofalo equation and the other derived from Avrami law.^[25] Again, the numerical method used for determining the constitutive equation consists of several steps of linearized regressions. A large amount of parameters must be determined.

Finally, a new approximation for modeling the constitutive equation based on differential equations is being developed.^[26-28] A set of internal variables is introduced usually in the differential Garofalo equation to obtain constitutive equations for a wide range of strains at high temperature. An additional constitutive differential equation is introduced for each internal variable. These internal variables describe the isotropic resistance to plastic flow, the softening due to recrystallization or the work hardening.^[29] The parameters are determined using integration of differential equations and not by means of optimization methods. This causes great complexity and requires a large amount of microstructural data.

The main objective of this work is to develop an explicit expression $\sigma(\varepsilon) = f(\varepsilon, T, \dot{\varepsilon})$, derived from the Garofalo equation, Eq. (1), that is able to reproduce stress-strain curves in a wide range of strains with a good statistical accuracy and to characterize the microstructural features of the plastic deformation of a magnesium alloy without the use of previous hypothesis.

II. EXPERIMENTAL PROCEDURE

Bars of AZ31 alloy were obtained by high temperature rolling. Composition of the magnesium alloy is given in Table 1.

A metallographic study was performed out in the as-received AZ31 alloy and in torsion-deformed samples to determine the structure and distribution of grain sizes.

A bimodal distribution is present in the AZ31 alloy in pre-torsioned samples. This distribution is typical of extruded materials that undergo partial DRX. The grain size in the transverse direction is larger than in the longitudinal direction. This is attributed to the radial extrusion component that causes a grain elongation.

The experimental data were obtained by means of torsion tests in a wide range of strain rates and temperatures. The torsion samples had an effective gage length of 50 mm and a radius of 3 mm. Strain rates in the range 0.71 to 8.73 s⁻¹ and temperatures in the range 575 to 728 K were used. Details of the hot torsion equipment have been given elsewhere.^[30]

The reduction process used was developed in previous studies.^[31-32] This consists of using a numerical algorithm that performs automatic conversion of torque, number of turns and speed of rotation, into true stress, deformation and true strain rate, respectively. We chose the von Mises method for the conversion. Determining the stress from the torque is usually performed with the Fields-Backofen equation:^[33]

$$\sigma = \frac{\sqrt{3}\Gamma}{2\pi R^3}(3 + \theta + m') \quad (2)$$

where σ is the stress, Γ is the torque, R is the radius of the torsion sample, and θ and m' are the work hardening and rate sensitivity of the torque respectively, which are defined as follows:

$$\theta = \left. \frac{\partial \ln \Gamma}{\partial \ln N} \right|_{\dot{N}, T} \quad m' = \left. \frac{\partial \ln \Gamma}{\partial \ln \dot{N}} \right|_{N, T} \quad (3,4)$$

where N is the number of turns and \dot{N} is the speed rotation.

This differential reduction method provides the functional dependence of both the strain rate sensitivity, m' , and the strain-hardening exponent, θ , with the number of turns, temperature and speed rotation. The functions $m = f(\dot{\varepsilon}, \varepsilon, T)$ and $\theta = f(\dot{\varepsilon}, \varepsilon, T)$ are important indicators of the characteristics of the processes governing creep. For instance, m is often about 0.5 and mostly in the range [0.4-0.6] for superplastic materials.^[34-35]

The hot torsion deformation of the alloy AZ31 is usually accompanied by adiabatic heating that is more pronounced at high strain rates and low temperatures.^[36,37] The softening related to adiabatic heating should be compensated to determine the influence of DRX processes that may occur in this material. The usual equation for the temperature rise with strain of the bulk material during deformation, ΔT , is the following:^[36]

$$\Delta T = \frac{\eta \int \sigma d\varepsilon}{\rho C} \quad (5)$$

where $\eta \in [0,1]$, is the Taylor-Quinney factor, ρ is the density and C is the specific heat. This correction has been achieved by applying a numerical algorithm.^[38] In the case of the alloy under study, AZ31, the density and specific heat are 1770 kg m^{-3} and $1190 \text{ J kg}^{-1} \text{ K}^{-1}$, respectively. The value taken for η is 0.9.^[39] The variation of specific heat with T is obtained as:

$$C = 0.0006 \cdot T^2 (\text{°C}) + 0.1978 \cdot T (\text{°C}) + 1028.2 \quad (6)$$

The adiabatic heating correction was conducted in two steps. The first step evaluated the temperature rise with bulk material straining, ΔT , as:^[36,40,41]

$$\Delta T = \frac{\eta}{\rho C} \int_0^\varepsilon \sigma_0^{wc}(s) ds \quad (7)$$

where σ_0^{wc} is the stress without adiabatic heating correction (directly from Fields-Backofen equation). The second step corrected the stress by the temperature rise effect using the following equation:^[42]

$$\sigma_0^c(\varepsilon, \dot{\varepsilon}, T) = \sigma_0^{wc}(\varepsilon, \dot{\varepsilon}, T) - \left. \frac{\partial \sigma_0^{wc}(T)}{\partial T} \right|_{\varepsilon, \dot{\varepsilon}} \Delta T \quad (8)$$

III. THE CONSTITUTIVE EQUATION

A general expression for the basic constitutive equation is the following:^[43]

$$\dot{\varepsilon} = f(\sigma, T, S_i, P_i) \quad (9)$$

where S_i are state variables and P_i are material constants. A particular strain dependent expression of this equation is the constitutive equation proposed in this work that is based on Eq. (1) and has the following form:

$$\dot{\varepsilon} = A(\varepsilon) e^{-\frac{Q(\varepsilon)}{RT}} \sinh^{n(\varepsilon)}(\alpha(\varepsilon) \cdot \sigma) \quad (10)$$

where A , Q , n and α are parameters that characterize the material.

Once all the stress-strain curves have been obtained and the effect of adiabatic heating has been corrected, a study of the best Garofalo equation was performed at strains in the range of 0.1 to 0.9, and at the peak stress. In torsion tests, the peak stress occurs at relatively high strains on the order of 0.45 for this material. We carried out the correction for adiabatic heating that guarantees a peak stress determination with minimal error. The objective is to determine the different values of the constants of the equation for a given strain. Its determination may characterize the phenomena underlying the plastic flow behavior of materials.^[44] The constitutive Eq. (10) is

determined at each strain by means of the Rieiro, Carsí, Ruano, RCR, method.^[45-47]
 Briefly, this method consists of linearizing the Garofalo equation in the form:

$$\ln(\dot{\varepsilon}) = \ln(A(\varepsilon)) - \frac{Q(\varepsilon)}{R \cdot T} + n(\varepsilon) \cdot \ln[\sinh(\alpha(\varepsilon) \cdot \sigma)] \quad (11)$$

The optimization of this equation is performed in the form of a hyperplane:

$$x_{3i} = \theta_0 + \theta_1 \cdot x_{1i} + \theta_2 \cdot x_{2i}(\theta_3) \quad (12)$$

where $\theta_0 = \ln(A)$ $\theta_1 = -Q$ $\theta_2 = n$ and $\theta_3 = \alpha$. A given plane is obtained at each $\theta_3 = \alpha$. Therefore, the best possible values of θ_0 , θ_1 and θ_2 can be obtained for a given value of θ_3 .

The minimum quadratic estimator of α is obtained by minimizing the sum of square errors, $S(\theta)$, $S(\theta) = \underline{e}' \cdot \underline{e} = (\underline{x}_3 - \underline{X})' \cdot (\underline{x}_3 - \underline{X})$ where $\underline{e}' = (\underline{x}_3 - \underline{X})'$ is the transposed expression for the errors of the fit.^[47] The result for this minimum is

$\underline{\theta} = (\underline{X}' \cdot \underline{X})^{-1} \cdot \underline{X}' \cdot \underline{x}_3$. Therefore, the variance and covariance of the estimators are

provided by the following matrix $Var(\underline{\theta}) = (\underline{X}' \cdot \underline{X})^{-1} \cdot \hat{\sigma}^2$ where $\hat{\sigma}^2 = \sum \frac{e_i^2}{(N - p)}$. The

total determination coefficient, R^2 , is obtained from the variance and covariance matrix. This coefficient has limitations as a quality parameter for the fit. Therefore, it is necessary to introduce the Fisher-Snedecor test. This test selects between two hypotheses. A favorable one where $\theta_0 = \theta_1 = \dots = \theta_{p-1} = 0$ and an alternative one where not all θ_i are zero, which means that the fit is good. High Fisher-Snedecor values correspond to a good fit. Therefore, this test produces an overall contrast of the data fit quality and the quality of the objective function.

Once the initial values are obtained a direct non linear regression procedure must be conducted based on the modified Gauss-Newton algorithm in order to obtain the optimal Garofalo equation.^[47] Changing notations and using $\{A, Q, n, \alpha\} =$

$\{\theta_1, \theta_2, \theta_3, \theta_4\}$ and $\underline{F}(\underline{\theta}) = \frac{\partial}{\partial \underline{\theta}'} f(\underline{\theta})$, the Garofalo equation is given as follows:

$$f(\underline{\theta}(\varepsilon), T, \sigma) = \theta_1(\varepsilon) \cdot e^{-\frac{\theta_2(\varepsilon)}{R \cdot T}} \cdot [\sinh(\theta_3(\varepsilon) \sigma)]^{\theta_4(\varepsilon)} \quad (13)$$

Finally, we use a Gauss-Newton method that simultaneously optimizes the four Garofalo parameters using the following algorithm:

$$\underline{\theta}_i = \underline{\theta}_{i-1} + (F^t(\underline{\theta}_{i-1}) \cdot F(\underline{\theta}_{i-1}))^{-1} \cdot F^t(\underline{\theta}_{i-1}) \cdot \left[\underline{y} - f(\underline{\theta}_{i-1}) \right] \quad (14)$$

where \underline{y} is the strain rate matrix.

IV. RESULTS AND DISCUSSION

Fig. 1 shows experimental data from torsion tests conducted at various temperatures and speed rotations. The data are given in the form of torque vs. number of turns before the reduction process.

The stress exponent, n , can be obtained from these data using the reduction procedure given in section 2. Fig. 2 shows n as a function of strain at various temperatures for the data given in Fig. 1a at 3.33 rps. The n values drop drastically at the beginning of deformation reaching a constant value, close to 2, at strains between 0.45 and 0.65. This is assumed to be the steady state regime. High stress exponents are observed at 575 K at high strains. This is typical of low temperature creep behavior where particles play an important role.

So far, the presence of a steady state is detected on hand of variations in the Garofalo equation parameters with strain, specially the parameter n as shown in Fig. 2. This presence is difficult to assess microstructurally because the torsion test must be stopped at certain strain values and the samples should be rapidly quenched to observe the microstructure.^[48] A further problem is the limited uniform deformation of the alloy and the presence of flow localization and void creation at strains close to those corresponding to steady state as shown in Fig. 3 and the rapid grain growth occurring at high temperature.

Fig. 3 shows true stress vs. true strain curves after the reduction process. This was performed in two stages. In the first stage, true stresses and true strains are obtained, in both cases, by means of the von Mises method,^[33,49] and in the second stage the stress

values were compensated considering the effect of adiabatic heating.^[38] The curves corrected for adiabatic heating are compared in the figure with those uncorrected. The average relative differences are about 7%. A strong drop in stress is observed after the peak value, which is attributed to the start of fracture. This impedes the development of a stress plateau corresponding to steady state.

The data at all temperatures and all strain rates are given in Table 2 for strains in the range of 0.1 to 0.8. It is now possible to construct strain rate vs. stress representations at any given strain and at various temperatures. Fig. 4 gives an example of these where $\varepsilon=0.4$ was selected.

The Garofalo equation was fitted to various strains along the stress-strain curve; the strains varied between values previous to the peak stress and those close to fracture. The fit was conducted in a wide range of strain rates and temperatures because it provides Garofalo parameters that are an average over all temperatures and strain rates. This can be done if the quality of the fit is supported by statistical parameters that guarantee its significance. A mathematical model, RCR, described in section 3 was used for the fit.^[47] We can now estimate the reproductive quality of the fit obtained with this model. Plots of the logarithm of the Zener-Hollomon parameter, Z , defined as $Z= \exp(Q/RT)$, versus the $\ln(\sinh(\alpha\sigma))$ term, used in the Garofalo equation (Eq. (1)), are shown in Fig. 5. This representation involves a grouping of thermal variables of the Garofalo equation, Q and T , into Z and on the other side the mechanical variable, σ . The figure indicates a good predictive capability.

This process can be applied for any given strain assuming a good statistical significance and sets of Garofalo equation parameters that can be obtained as a function of strain. Therefore, an implicit strain dependent equation, a modified Garofalo equation, can be expressed as given in Eq. (10).

It should be noted that the application of the RCR method does not require that stress-strain curves exhibit an extended plateau. This is because the functions representing the variation of the four Garofalo parameters with strain show this state, when it exists. The following equation allows representations of stress-strain curves by inverting the independent variables:

$$\sigma = \frac{1}{\alpha(\varepsilon)} \cdot \sinh^{-1} \left\{ \left(\frac{\dot{\varepsilon} \cdot e^{\frac{Q(\varepsilon)}{R \cdot T}}}{A(\varepsilon)} \right)^{1/n(\varepsilon)} \right\} \quad (15)$$

The explicit dependence of strain rate and temperature on stress of Eq. (15) allows reproduction of each curve that was used to obtain the Garofalo parameters. It should be noted that we do not conduct an explicit functional fit of the Garofalo parameters. In our procedure we use, for a given strain, the set of four parameters obtained for that particular strain; therefore, Eq. (10) is inverted numerically for any given strain. As a consequence, a good fit of a curve at a given strain rate and temperature must be attributed to the goodness of the modified Garofalo equation in physically describing the deformation process. Otherwise, only the curves in the middle range of temperatures and strain rates would be reproduced correctly. The accuracy in the reproducibility of the stress-strain curves must be attributed to the explicit dependence of the stress on strain rate and temperature in Eq. (15).

Eq. (15) can be modified to a more suitable expression using, i) a normalized Zener-

Hollomon expression of the form $Z^*(\dot{\varepsilon}, T, \varepsilon) = \left(\frac{\dot{\varepsilon} \cdot e^{\frac{Q(\varepsilon)}{R \cdot T}}}{A(\varepsilon)} \right)^{\frac{1}{n(\varepsilon)}}$ and ii) the classical

expression for $\sinh^{-1}(x) = \ln(x + \sqrt{x^2 + 1})$. This leads to the following equation:

$$\sigma(\varepsilon) = \frac{\ln(Z^*(\dot{\varepsilon}, T, \varepsilon) + \sqrt{(Z^*(\dot{\varepsilon}, T, \varepsilon))^2 + 1})}{\alpha(\varepsilon)} \quad (16)$$

This concept can be now applied to the deformation behavior of AZ31 magnesium alloy that was deformed in torsion at various temperatures and strain rates. Table 3 gives the fitted values of the Garofalo parameters for some strains obtained by the RCR method. The last two columns of Table 3 give two statistical parameters used to verify the significance of each fit. These are the Fisher-Snedecor function, F , and the determination coefficient, R^2 . Table 3 gives values of the Garofalo parameters for eight different strains in the range 0.1 to 0.8.

It could be thought that the evolution of the parameters $\{A(\varepsilon), Q(\varepsilon), n(\varepsilon), \alpha(\varepsilon)\}$ with strain is random and therefore Eq. (15) would not be a constitutive equation. To prove that this is not the case, multiple fits for different mathematical expressions for describing the evolution of each Garofalo parameter with strain have been tried. The best fit is described by the following equations:

$$1000\alpha(\varepsilon)=26.414 - 48.421 \varepsilon + 106.5 \varepsilon^2 - 81.894 \varepsilon^3 \quad R^2 = 0.98 \quad (17)$$

$$n(\varepsilon)=3.78 + 0.019 \varepsilon - 9.235 \varepsilon^2 + 8.639 \varepsilon^3 \quad R^2 = 0.99 \quad (18)$$

$$Q(\varepsilon)=133.725+135.264 \varepsilon - 458.078 \varepsilon^2 +243.788 \varepsilon^3 \quad R^2 = 0.99 \quad (19)$$

$$\ln(A(\varepsilon))=26.563 + 8.870 \varepsilon - 58.980 \varepsilon^2 + 37.568 \varepsilon^3 \quad R^2 = 0.98 \quad (20)$$

These equations have no predictive capability and are only used to statistically measure the functional behavior of the parameter dependence on strain. This means that a new set of values for the Garofalo parameters would not be generated by these equations since very significant differences exist with respect to the experimental curves and to those generated by the proposed constitutive equation. The very high values of the determination coefficients, and the fact that the best fit is the same for the four parameters, indicate that the dependence of the Garofalo parameters with strain is not random but, in contrary, represents a functionally significant behavior.

Some considerations on the statistical quality of our model should be given. This can be done by considering the values of the coefficient of determination and of the statistical parameter of Fisher-Snedecor given in Table 3. The evolution of both statistical parameters is given in Fig. 6. The F parameter is a statistical value verifying

the following probability relation $P(\xi_F > F) = \int_F^{+\infty} f(\xi_F) \cdot d\xi_F$ where $f(\xi_F)$ is a density

of probability function of Fisher-Snedecor associated to the null hypothesis for the test about the validity of the proposed model. When a given confidence is fixed, for instance, 0.95, the admissible error has a value of 0.05. Then, for a bidirectional contrast, the model is acceptable with a confidence of 95% if $P(\xi_F > F) < 0.025$. In our case, the model has a good predictive capability at strains between 0.2 and 0.8 with

the optimal predictive region between 0.4 and 0.7. The percentage of variance explained by the model is higher than 90 % in this strain interval. However, the error is significant for strains lower than 0.2.

The values given in Table 3 are plotted as a function of strain in Fig. 7. This figure shows a clear dependence of the four Garofalo parameters with strain for the AZ31 alloy. Fig. 7a shows the functional relation of the parameter α with strain. The first strain regime is associated with work hardening and the beginning of softening due to dynamical recovery or incipient dynamical recrystallization. This regime extends to strains up to about 0.35 and corresponds to the strains close to peak stresses in the stress – strain curves. For larger strains, a quasi-stationary region is observed. The alpha parameter shows a 20% decrease at about $\varepsilon=0.5$ which could be related to DRX and its effect on grain size. In this region, strain hardening is balanced by the softening due to DRX that continues for strains of about 0.7. The further decrease is associated with flow localization and mechanical instability mechanisms. Figure 7b shows the variation of the activation energy with strain. A value of about 145 kJ/mol is obtained at strains close to the peak diminishing to 115 kJ/mol at $\varepsilon=0.5$; the peak corresponds to the plateau region of the alpha parameter. However, the Q values further decrease at higher strains and Q is close to 90 kJ/mol at $\varepsilon=0.7$. This decrease must be attributed first to a softening process, probably due to DRX and grain size refinement and then to the mentioned flow localization. On the other hand, the stress exponent n decreases from values close to 3.7 to 2.8 at $\varepsilon=0.4$, see Fig. 7c. The values are smaller than that corresponding to a slip creep power law model where $n=5$. These values are, however, similar to those obtained by other authors for the same alloy when the data is refined of the data is conducted.^[36] Again, the n variation is attributed to changes in the microstructure due to DRX and grain refinement. The evolution of n shows an apparent stationary state at strains between 0.5 and 0.8. This coincides with the results given in Fig. 2. A minimum n value of 2.28 at $\varepsilon=0.71$ is obtained by assuming a cubic function for the evolution of n with strain in the temperature and strain rates ranges considered.

Finally, Fig. 7d shows the decrease of A with strain down to $\varepsilon=0.5$ that is related to the softening process. The further decrease at higher strains can be related to flow localization. This decreasing trend is clear and statistically significant, with $R^2 = 0.98$.

indicating that it is not a random process. The evolution of $\ln A$ with strain is contrary to that occurring in other materials.^[32,45,46]

The adiabatic heating correction may strongly influence the results at high strains. This should be considered when comparing the uncorrected data of some authors. However, at low strains the agreement is usually better.

It is worth noting that DRX takes place during deformation of the AZ31 alloy at all temperatures and strain rates investigated. Examples of the microstructures before and after torsion deformation ($419^\circ\text{C}/2\text{s}^{-1}$) are given in Figs. 8a and b, respectively. Both micrographs correspond to longitudinal sections. The grain size of the deformed sample is finer than that before deformation, 27 vs 33 μm according to the linear intercept method, ASTM112, and equiaxed grains are observed. In addition, the bimodal grain structure of the sample before testing, similar to that described by Spigarelli et al.,^[50] is partially removed in the deformed samples, i.e., the grain size distribution of the deformed samples is more homogeneous. These are indications that DRX occurs along deformation. The sample was not quenched after the test and probably some grain growth occurred after the sample fractured. Furthermore, according to McQueen et al.^[51] the strong drop after the peak stress is attributed to melting of segregated phases at the grain boundaries. This may cause a second and local adiabatic heating that may lead to flow localization and void growth.

Our results can be compared with those obtained by other authors. First, we emphasize various studies that agree with our results in many aspects. The group of McQueen obtained similar values of $Q = 140$ kJ/mol in the range 513 to 573 K at 1 s^{-1} which they related to dislocation climb of basal dislocations.^[52] Spigarelli et al., working at peak stresses, reported $n = 4$, and $\alpha = 0.02 \text{ MPa}^{-1}$ in agreement with our results.^[50] These authors obtained $Q = 155$ kJ/mol in the same temperature range, which they associated with two possible diffusivities, that for self-diffusion in magnesium, 135 kJ/mol, and diffusion of aluminum in the magnesium matrix, $Q = 143$ kJ/mol. On the other hand, Takuda et al. reported $Q = 136$ kJ/mol in the same range of temperatures and lower strain rates^[53] and Dong and Ying gave similar values for n and α and obtained slightly higher values of Q , 160 kJ/mol.^[26] Tan and Tan reported n values of about 2.5 for the steady state close to our values.^[54] Barrett showed $Q = 147$ kJ/mol at low strains and about 92 kJ/mol for $\varepsilon = 0.6$.^[43] This is in agreement with the results of Somekawa et

al. ^[55], Kim et al. ^[56] and del Valle et al. ^[57] The low activation energy values are attributed to a slip creep mechanism controlled by pipe diffusion.

In contrast, we found studies that contain differences with respect to our results that should be analyzed. Li et al. studied the evolution of the Garofalo parameters with strain from stress-strain curves corrected by adiabatic heating. ^[36] These authors found an increase of n with strain in the region where DRX takes place, which is contrary to expectations. Probably the authors used numerical methods that are inappropriate and these cannot be validated since a statistical analysis of accuracy is missing. McQueen et al. reported at the peak stress, a high $\alpha \approx 0.05 \text{ MPa}^{-1}$, for 573 K and strain rates of 0.3, 0.1, and 1 s^{-1} . ^[58] However, the authors obtained a steady state at $\varepsilon=0.5$ showing n of about 5.5 and activation energies of about 148 kJ/mol.

We have so far discussed the evolution of the Garofalo parameters with strain. This evolution can be used to build an equation for the AZ31 alloy, similar to Eq. (10), but it must be established if it is a constitutive equation. It is our contention that a constitutive equation must fulfill two conditions: i) it should be able to characterize the flow behavior in a given strain rate and temperature range and ii) it should be able to reproduce stress-strain curves with high statistical quality.

Two kinds of data can be used to characterize the flow behavior of the AZ31 alloy. On one hand, data related to the evolution of the Garofalo parameters with strain and on the other hand, data characterizing the evolution of the microstructure linked to DRX of the alloy. In Table 4 we present the strain values that characterize the critical points of the fitting functions, Eqs. (17) to (20), describing the evolution of the Garofalo parameters with strain. ε_{\min} is the strain for the minimum of the functional relation, ε_{\max} is the strain for the maximum of the functional relation, and ε_{inf} is the strain for the inflection point of the functional relation. We intend to show that a strong correlation exists between these critical values that characterize the changes in the evolution of the stress-strain curves and the parameters characterizing DRX for this material. The DRX process is the main softening mechanism in this alloy for the analyzed range. Consequently, we want to show that the strain dependent constitutive equation, Eq. (10), supplies critical values of strain linked to critical values of DRX. The critical values of the constitutive equation are obtained from the functional dependence of the Garofalo parameters with strain. On the other hand, from various investigations

[8,24,36,54,59,60] we selected the characteristic values that are more representative of the DRX processes in the AZ31 magnesium alloy in the temperature range of our work. These values are shown in Table 5. ε_s is the strain for initial formation of sub grains, ε_{drx} is the strain for initial dynamic recrystallization, ε_p is the strain for the average peak and ε_{50} is the strain for 50% of recrystallized volume fraction.

The critical points given in Tables 4 and 5 are shown in the curves representing the four Garofalo parameters as a function of strain in Fig. 9. It can be observed that the strain for the start of subgrain formation is similar to the strains at which the activation energy Q and $\ln(A)$ reach their maximum values. We can also observe that the inflection point for α and $\ln(A)$ functions in Fig. 9 is close to the average strain value for the peaks of the stress-strain curves, which is about 0.45. It is also very significant that the value of strain for which the material reached the 50% recrystallized volume fraction is close to those values at which n and $\ln(A)$ reached their minimum value, and the Q function reached their inflection point.

We can also observe that the alpha parameter reaches certain stability as soon as DRX is progressing. In addition, the end of the stability zone of α is close to the strain value at which 50 % recrystallization is reached. At higher strains, flow localization and cavitation take place. The stability interval corresponds to strains in the range of 0.3 to 0.6. This shows that the possible stability in the microstructure does not have to coincide with the apparent stability of the stress strain curves.

A new constitutive equation, Eq. (10), is proposed in this work. It is important to verify the predictive capacity of this equation. Table 3 values can be used to reproduce stress-strain curves according to Eqs. (15) or (16). Plots of predicted and experimental values for the AZ31 alloy are given in Fig. 10 at various temperatures and two strain rates, 0.73 s^{-1} , Fig. 10a, and 2.00 s^{-1} , Fig. 10b. The agreement is quite good and the average relative error is about 6.5 %. For $\dot{\varepsilon}=0.73 \text{ s}^{-1}$ and 2.00 s^{-1} the relative average errors are 4.5 % and 6.4%, respectively. For $\dot{\varepsilon}=8.71 \text{ s}^{-1}$, not shown in the figure, this error is 8.7%, giving a mean value of errors of 6.9%. This effect should not be attributed to the quality of the proposed model but to the experimental error that increases with increasing torsion rates.

Finally, the relative error for prediction of our model can be contrasted with the relative errors of other models. For instance, Takuda et al.^[53] showed relative errors of

about 25 %, Cho et al. ^[20] of about 13%, and Maksoud et al. ^[61] of about 8%. Other investigations in modeling using constitutive equations do not allow error determinations. ^[26,36] We can therefore conclude that the average relative errors shown in this work are better than those reported in the literature.

The equation developed in this work is a good constitutive equation with predictive capability and physical meaning. It is worth noting that the stress-strain curves can be reproduced with better accuracy, on the order of 4%, using only numerical methods, for instance, by neuronal networks.^[4] However, these are fitting models without any physical meaning. In contrast, our proposed constitutive equation containing four parameters provides elements that allow the description and analysis of the deformation behavior of materials. Furthermore, the model may be used to describe the evolution of average microstructural parameters. For this purpose, additional equations relating the strain dependent Garofalo parameters with the microstructure are needed.

V. SUMMARY

A new strain dependent constitutive equation has been developed to describe the stress-strain curves of materials. This equation has a high prediction capability with a low average error of prediction. The evolution of the parameters for the new equation as a function of strain allows comparison of experimental data with predictions provided by this new equation. This equation also describes the microstructural changes occurring during deformation of the AZ31 magnesium alloy. This equation is able to describe the effects of microstructural changes occurring during deformation of the AZ31 magnesium alloy. However, additional equations relating the strain dependent Garofalo parameters with the microstructure are needed.

ACKNOWLEDGEMENTS

The authors would like to thank financial support of Projects PET2007-0475 and MAT2006-13348 from CICYT, Spain. We thank Victor López and the Metallographic Laboratory from CENIM for their help with the optical micrographs.

REFERENCES

1. R. Ebrahimi, S.H. Zahiri, and A. Najafizadeh: *J. Mater. Processing Technol.*, 2006, vol. 171, pp. 301-305.
2. X.-Y Diao, H.-W Luo, R.-Z Wang, and J.-Z Xiang: *J. Iron Steel Res. Int. Inter.*, 2007, vol. 14, pp. 335-338.
3. I. Rieiro, M. Carsí, and F. Peñalba: *Rev. Metal. Madrid*, 1996, vol. 32, pp. 321-328.
4. M. Zhou and M.P. Clode: *Mech. Mater.*, 1998, vol. 27, pp. 63-76.
5. Z. Yang, Y.C. Guo, J.P. Li, F. He, F. Xia, and M.X. Liang: *Mater. Sci. Eng. A*, 2008., vol. 485, pp. 487-491.
6. H. Sakasegawa, S. Ukai, M. Tamura, S. Ohtsuka, H. Tanigawa, H. Ogiwara, A. Kohyama, and M. Fujiwara: *J. Nuclear Mater.*, 2008, vol. 373, pp. 82-89.
7. S.M. Abbasi and A. Shokuhfar: *Mater. Lett.*, 2007, vol. 61, pp. 2523-2526.
8. X. Duan and T. Sheppard: *J. Mater. Process. Technol.*, 2004, vol. 150, pp. 100-106.
9. B. Rønning and N. Ryum: *Metall. Mater. Trans. A*, 2001, vol. 32A, pp. 769-776.
10. H. Luthy, A.K. Miller, and O.D. Sherby: *Acta Metall.*, 1980, vol. 28, pp. 169-178.
11. A. Cingara and H.J. McQueen: *J. Mater. Process. Technol.*, 1992, vol. 36, pp. 17-30.
12. J.J. Urcola and C.M. Sellars: *Acta Metall.*, 1987, vol. 35, pp. 2637-2647.
13. J.C.M. Li: *Trans. AIME*, 1963, vol. 227, pp. 1474-1477.
14. I. Rieiro, J. Castellanos, J. Muñoz, V. Gutierrez, M. Carsí, and O.A. Ruano: *Proc. X Congreso Nacional de Materiales, San Sebastián*, 2008, vol. 1, pp. 317-321.
15. F.R.N Nabarro: *Acta. Mater.*, 2006, vol. 54, pp. 263-295.
16. K. Kannan, C. Hamilton, and C. Johnson: *Metall. Mater. Trans. A*, 1998, vol. 29, pp. 1211-1220.
17. H.J. McQueen: *Metall. Mater. Trans. A*, 2002, vol. 33A, pp. 345- 362.

18. Y.C. Lin, M.S. Chen, and J. Zhang: *Mater. Sci. Eng. A*, 2009. vol. 499, pp. 88-92.
19. W.M. van Haaften, B. Magnin, W.H. Kool, and L. Katgerman: *Metall. Mater. Trans. A*, 2002, vol. 33A, pp. 1971-1980.
20. J.R. Cho, W.B. Bae, W.J. Wang, and P. Hartley: *J. Mater. Process. Technol.*, 2001, vol. 118, pp. 356-361.
21. W. Wei, K.X. Wei, and G.J. Fan: *Acta Mater.* 2008, vol. 56, pp. 4771-4779.
22. E.S. Puchi-Cabrera: *Metall. Mater. Trans. A*, 2003, vol. 34A, pp. 2837-2846.
23. M. Militzer and Y. Brechet: *Metall. Mater. Trans. A*, 2009, vol. 40A, pp. 2273-2282.
24. M.P. Phaniraj and A.K. Lahiri: *Mater. Design*, 2008, vol. 29, pp. 734-738.
25. M. Zhou and M.P. Clode: *J. Mater. Process. Technol.*, 1991, vol. 72, pp. 78-85.
26. H.-X Dong and J.-D. Ying: *Trans. Nonferrous Metall. Soc. China*, 2006, vol. 16, pp. 586-590.
27. S.B. Brown, K.H. Kim, and L. Anand: *Int. J. Plasticity*, 1989, vol. 5, pp. 95-130.
28. J. Lin and Y. Liu: *J. Mater. Process. Technol.*, 2003, vol. 143-144, pp. 281-285.
29. H. Luo, J. Sietsma, and S. van der Zwaag: *Metall. Mater. Trans. A*, 2004, vol. 35A, pp. 1889-1898.
30. I. Rieiro, J. Castellanos, J. Muñoz, M. T. Larrea, V. Amigo, and O.A. Ruano: *Proc. XI Congreso Nacional de Tratamientos Térmicos y de Superficie*, Valencia, Spain, 2008, pp. 175-189.
31. J. Castellanos, I. Rieiro, J. Muñoz, M. Carsí, and O.A. Ruano: *Proc. IX Congreso Nacional de Materiales*, Vigo, Spain, 2006, pp. 211-214
32. J. Castellanos, I. Rieiro, M. Carsí, J. Muñoz, and O.A. Ruano: *J. Achievements Mater. Manufacturing Eng.*, 2006, vol. 18, pp. 447-454.
33. D.S. Fields, W.A. Backofen: *Proc. ASTM*, 1957, vol. 57, pp. 1259-1272.
34. J. Pilling and N. Ridley: *Superplasticity in crystalline solids*, The Institute of Metals, London, UK, 1989.
35. M.A. Nazzal, M. K. Kraisheh, and F.K. Abu-Farha: *J. Mater. Process. Technol.*, 2007, vol. 191, pp. 189-192.
36. L. Li, J. Zhou, and J. Duszczek: *J. Mater. Process. Technol.*, 2006, vol. 172, pp. 372-380.

37. H. Monajati, M. Jahazi, S. Yue, and A.K. Taheri: *Metall. Mater. Trans. A*, 2005, vol. 36A, pp. 895-905.
38. J. Castellanos, I. Rieiro, M. Carsí, J. Muñoz, and O.A. Ruano: *WIT Trans. Eng. Sci.*, 2007, vol. 57, pp. 219-228.
39. A. Bhattacharyya, D. Rithel, and G. Ravichandran: *Metall. Mater. Trans. A*, 2006, vol. 37, pp. 1137-1145.
40. W. Pantleon, D. Francke, and P. Klimanek: *Computational Mater. Sci.*, 1996, vol. 7, pp. 75-81.
41. R. Kapoor and S. Nemat-Nasser: *Mech. Mater.* 1998, vol. 27, pp.1-12.
42. J. Castellanos, I. Rieiro, M. Carsí, J. Muñoz, M. El Mehtedi, and O.A. Ruano: *Mater. Sci. Eng. A*, 2009, vol. 517, pp. 191-196.
43. M.R. Barrett: *J. Light Met.*, 2001, vol. 1, pp. 167-177.
44. H.J. McQueen and N.D. Ryan: *Mater. Sci. Eng. A*, 2002, vol. 322, pp. 43-63.
45. I. Rieiro: Ph D Thesis, UCM, Madrid, Spain, 1997.
46. I. Rieiro, O.A. Ruano, M. Eddahbi and M. Carsi: *J. Mater. Process. Technol.*, 1998, vol. 78, pp. 177-183.
47. I. Rieiro, M. Carsí, and O.A. Ruano: *Mater. Sci. Technol.*, 2009, vol. 25, pp. 995-1002.
48. S.-H. Choi, J.K. Kim, B.J. Kim, and Y.B. Park: *Mater. Sci. Eng. A*, 2008, vol. 488, pp.458-467.
49. E. Lach and K. Pöhlandt, *J. Mechanical Working Technol.*, 1984, vol. 9, pp. 67-80.
50. S. Spigarelli, M. El Mehtedi, M. Cabiddo, E. Evangelista, J. Kaneko, A. Jäger, and V. Gartnerova: *Mater. Sci. Eng. A*, 2007, vol. 462, pp. 197-201.
51. A. Mwembela, E.B. Konopleva, and H.J. McQueen: *Scripta Mater.*, 1997, vol. 37, pp. 1789-1795.
52. M.M. Myshlyaev, H.J. McQueen, A. Mwembela, and E. Konopleva: *Mater. Sci. Eng. A*, 2002, vol. 337, pp. 121-133.
53. H. Takuda, H. Fujimoto, and N. Haifa: *J. Mater. Process. Technol.*, 1998, vol. 80-81, pp. 513-516.
54. J.C. Tan and M.J. Tan: *Scripta Mater.*, 2002, vol. 47, pp. 101-106.
55. H. Somekawa, K. Hirai, H. Watanabe, Y. Takigawa, and K. Higashi: *Mater. Sci. Eng. A*, 2005, vol. 407, pp. 53-61.

56. W.J Kim, S.W. Chung, C.S. Chung, and D. Kum: *Acta Mater.*, 2001, 49, pp. 3337–3345.
57. J.A. del Valle, M.T. Pérez-Prado, and O.A. Ruano: *Metall. Mater. Trans. A*, 2005, vol. 36A, pp. 1427-1438.
58. H.J. McQueen, M.M. Myshlaev, M. Sauerborn, and A.M. Mwembela: in *Magnesium Technology 2000*, H.I. Kaplan, J.N. Hryn, and B.B. Clow, eds., TMS, Warrendale, PA, 2000, pp. 355-362.
59. A.G. Beer and M.R. Barnett: *Mater. Sci. Eng. A*, 2006, vol. 423, pp. 292-295.
60. B.H. Lee, N.S. Reddy, J.T. Yeom, and C.S. Lee: *J. Mater. Process. Technol.*, 2007, vol. 187-188, pp. 766-769.
61. I.A. Maksoud, H. Ahmed, and J. Rödel: *Mater. Sci. Eng. A*, 2009, vol. 504, pp. 40-48.

Al	Zn	Si	Cu	Mn	Fe	Ni	Ca	Zr	Mg
2.8	0.92	0.01	<0.001	0.22	0.002	<0.001	<0.01	<0.001	Bal.

Table 1. Nominal composition of the AZ31 magnesium alloy (wt. %).

ϵ	σ [MPa]	$\dot{\epsilon}$ [s^{-1}]	T, K	ϵ	σ [MPa]	$\dot{\epsilon}$ [s^{-1}]	T, K	ϵ	σ [MPa]	$\dot{\epsilon}$ [s^{-1}]	T, K	ϵ	σ [MPa]	$\dot{\epsilon}$ [s^{-1}]	T, K
0.1	16.47	0.726	728	0.2	21.87	0.726	728	0.3	24.58	0.726	728	0.4	25.37	0.726	728
0.1	24.79	0.726	690	0.2	34.56	0.726	690	0.3	38.03	0.726	690	0.4	39.65	0.726	690
0.1	33.96	0.726	648	0.2	45.30	0.726	648	0.3	51.26	0.726	648	0.4	52.51	0.726	648
0.1	52.33	0.726	604	0.2	70.47	0.726	604	0.3	78.87	0.726	604	0.4	82.01	0.726	604
0.1	65.15	0.726	575	0.2	87.48	0.726	575	0.3	99.46	0.726	575	0.4	103.31	0.726	575
0.1	25.61	8.706	728	0.2	38.65	8.706	728	0.3	46.23	8.706	728	0.4	54.50	8.706	728
0.1	31.47	8.706	690	0.2	47.21	8.706	690	0.3	56.82	8.706	690	0.4	63.22	8.706	690
0.1	54.07	8.706	648	0.2	76.83	8.706	648	0.3	90.51	8.706	648	0.4	101.69	8.706	648
0.1	78.30	8.706	604	0.2	106.36	8.706	604	0.3	119.44	8.706	604	0.4	129.61	8.706	604
0.1	69.65	8.706	575	0.2	102.23	8.706	575	0.3	123.01	8.706	575	0.4	137.30	8.706	575
0.1	19.34	2.000	728	0.2	26.91	2.000	728	0.3	31.74	2.000	728	0.4	32.48	2.000	728
0.1	28.78	2.000	690	0.2	37.95	2.000	690	0.3	44.01	2.000	690	0.4	45.55	2.000	690
0.1	40.84	2.000	648	0.2	54.30	2.000	648	0.3	62.42	2.000	648	0.4	65.63	2.000	648
0.1	66.66	2.000	604	0.2	86.06	2.000	604	0.3	98.51	2.000	604	0.4	104.27	2.000	604
0.1	74.42	2.000	575	0.2	101.53	2.000	575	0.3	118.38	2.000	575	0.4	126.86	2.000	575
ϵ	σ [MPa]	$\dot{\epsilon}$ [s^{-1}]	T, K	ϵ	σ [MPa]	$\dot{\epsilon}$ [s^{-1}]	T, K	ϵ	σ [MPa]	$\dot{\epsilon}$ [s^{-1}]	T, K	ϵ	σ [MPa]	$\dot{\epsilon}$ [s^{-1}]	T, K
0.5	24.73	0.726	728	0.6	21.81	0.726	728	0.7	19.53	0.726	728	0.8	16.72	0.726	728
0.5	39.01	0.726	690	0.6	36.51	0.726	690	0.7	32.81	0.726	690	0.8	28.51	0.726	690
0.5	52.02	0.726	648	0.6	47.10	0.726	648	0.7	40.33	0.726	648	0.8	33.58	0.726	648
0.5	81.57	0.726	604	0.6	74.92	0.726	604	0.7	63.72	0.726	604	0.8	49.52	0.726	604
0.5	103.35	0.726	575	0.6	94.59	0.726	575	0.7	78.83	0.726	575	0.8	57.35	0.726	575
0.5	55.87	8.706	728	0.6	54.16	8.706	728	0.7	49.96	8.706	728	0.8	43.43	8.706	728
0.5	65.34	8.706	690	0.6	63.73	8.706	690	0.7	59.06	8.706	690	0.8	50.23	8.706	690
0.5	107.03	8.706	648	0.6	107.09	8.706	648	0.7	98.50	8.706	648	0.8	84.01	8.706	648
0.5	133.73	8.706	604	0.6	126.57	8.706	604	0.7	122.50	8.706	604	0.8	111.04	8.706	604
0.5	144.70	8.706	575	0.6	144.83	8.706	575	0.7	133.92	8.706	575	0.8	112.26	8.706	575
0.5	31.55	2.000	728	0.6	28.10	2.000	728	0.7	24.60	2.000	728	0.8	19.91	2.000	728
0.5	45.14	2.000	690	0.6	41.04	2.000	690	0.7	36.09	2.000	690	0.8	29.73	2.000	690
0.5	64.93	2.000	648	0.6	61.12	2.000	648	0.7	54.54	2.000	648	0.8	44.70	2.000	648
0.5	104.36	2.000	604	0.6	95.87	2.000	604	0.7	78.83	2.000	604	0.8	55.77	2.000	604
0.5	127.87	2.000	575	0.6	121.43	2.000	575	0.7	104.02	2.000	575	0.8	77.81	2.000	575

Table 2. Reduced data for strain, stress, strain rate and temperature corrected for adiabatic heating at various strains.

ε	$\log(A)$	Q , kJ/mol	n	α (x1000)	F	R^2
0.1	26.747	141.42	3.700	22.27	9.7	0.620
0.2	26.340	146.11	3.446	20.93	25.4	0.809
0.3	25.709	143.96	3.293	19.20	50.3	0.894
0.4	22.159	124.28	2.774	18.67	69.8	0.921
0.5	20.845	115.95	2.575	18.00	86.0	0.935
0.6	19.019	104.68	2.316	18.53	95.1	0.941
0.7	17.020	89.73	2.275	16.80	92.1	0.939
0.8	14.962	72.09	2.290	13.73	51.5	0.896

Table 3. Fit of the Garofalo parameters at various strains for the AZ31 alloy.

Parameter	ε_{\min}	ε_{\max}	ε_{\inf}
α			0.43
Q		0.1500	0.63
n	0.71	0.0004	0.36
$\ln(A)$	0.97	0.0810	0.52

Table 4. Strain critical values that characterized the functional dependence of the Garofalo equation parameters with strain for AZ31 magnesium alloy.

ε_{is}	ε_{dix}	ε_p	ε_{50}
0.12	0.21	0.45	0.68

Table 5. Average dynamic recrystallization parameters for the AZ31 magnesium alloy.

FIGURE CAPTIONS

Figure 1. Digitized curves of torque vs. number of turns in experimental torsion tests for the magnesium AZ31 alloy at various temperatures and at three speed rotations, 3.33, 9.18 and 40 rps.

Figure 2. Evolution of stress exponent with strain at 0.73 s^{-1} and various temperatures for the AZ31 magnesium alloy.

Figure 3. Stress-strain curves for all temperatures and strain rates, with and without adiabatic heating correction. Uncorrected curves are marked with U and the corrected dashed ones with C.

Figure 4. Strain rate as a function of flow stress for $\varepsilon=0.4$ at various temperatures for the AZ31 alloy.

Figure 5. Relationship between the Zener-Hollomon parameter and the stress at $\varepsilon=0.4$ for the AZ31 alloy. The continuous line is the fit obtained with the Garofalo parameters, given in the figure, obtained by the RCR model and the dashed lines are the upper and lower limits for the confidence intervals attributed to the predicted results.

Figure 6. Strain dependence of statistical parameters controlling the model quality.

Figure 7. Representation of the four Garofalo parameters as a function of strain for the AZ31 alloy. The continuous line in each subplot corresponds to the best fit. The equations used for the fit are given in the figure legends.

Figure 8. Micrographs of AZ31 alloy obtained (a) before torsion testing and (b) after torsion testing at $419^{\circ}\text{C}/2 \text{ s}^{-1}$.

Figure 9. Variation of parameters of Garofalo equation with strain. The principal strain values that characterize the microstructural evolution of the AZ31 alloy are indicated. Tables 4 and 5 define the strains given in the graphs.

Figure 10. Strain-stress curves from experimental data (continuous lines) and from model predictions (dashed lines) at various temperatures at (a) 0.73 s^{-1} , (b) 1.99 s^{-1} and (c) 8.71 s^{-1} .

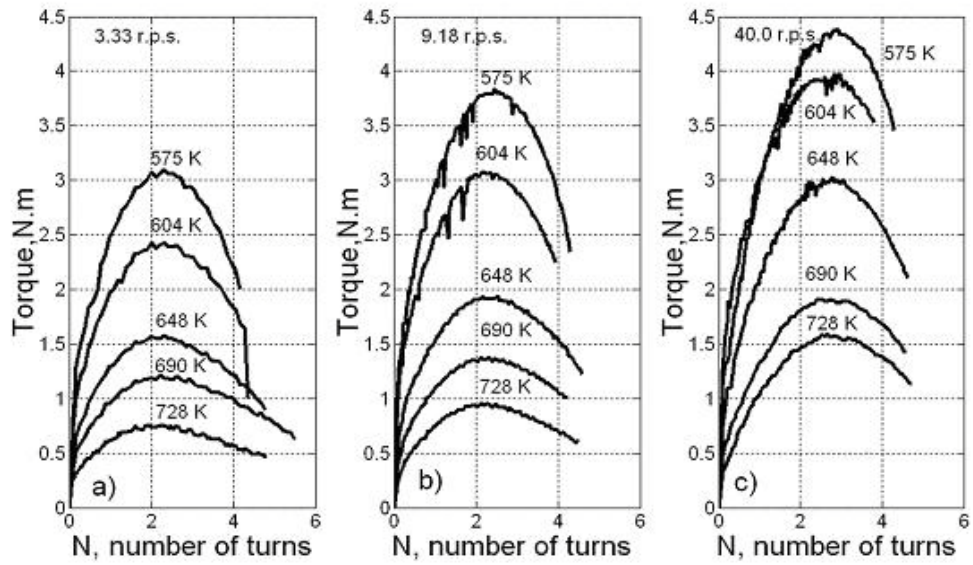


Figure 1. Digitized curves of torque vs. number of turns in experimental torsion tests for the magnesium AZ31 alloy at various temperatures and at three speed rotations, 3.33, 9.18 and 40 rps.

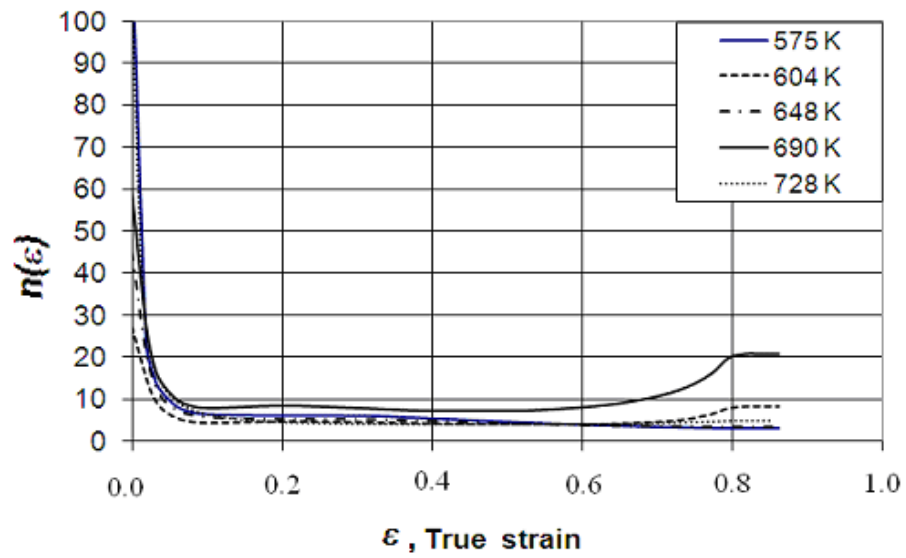


Figure 2. Evolution of stress exponent with strain at 0.73 s^{-1} and various temperatures for the AZ31 magnesium alloy.

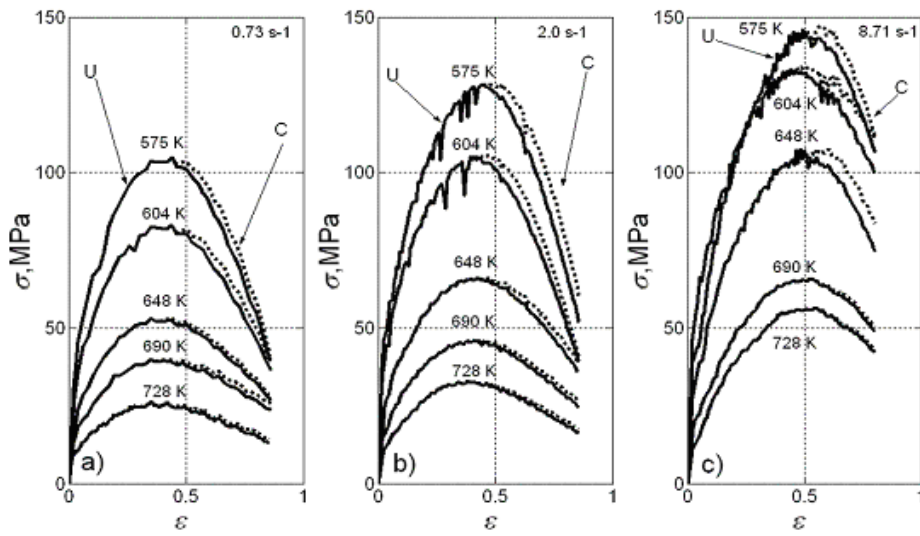


Figure 3. Stress-strain curves for all temperatures and strain rates, with and without adiabatic heating correction. Uncorrected curves are marked with U and the corrected dashed ones with C.

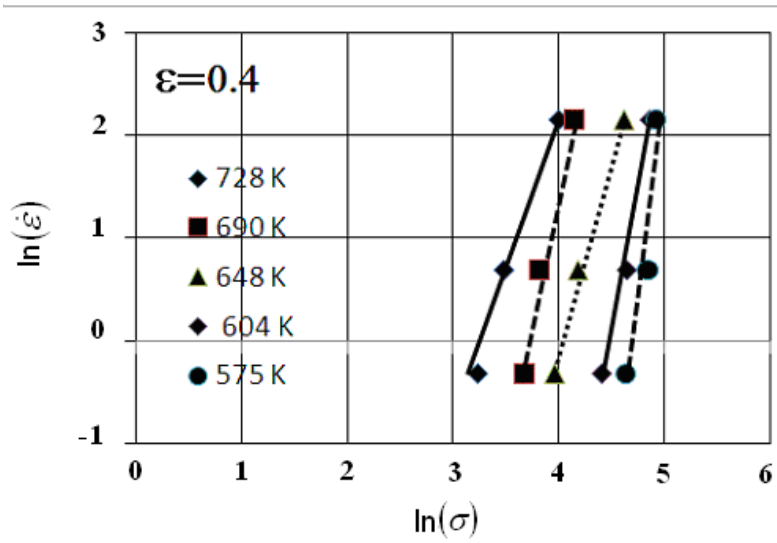


Figure 4. Strain rate as a function of flow stress for $\epsilon=0.4$ at various temperatures for the AZ31 alloy.

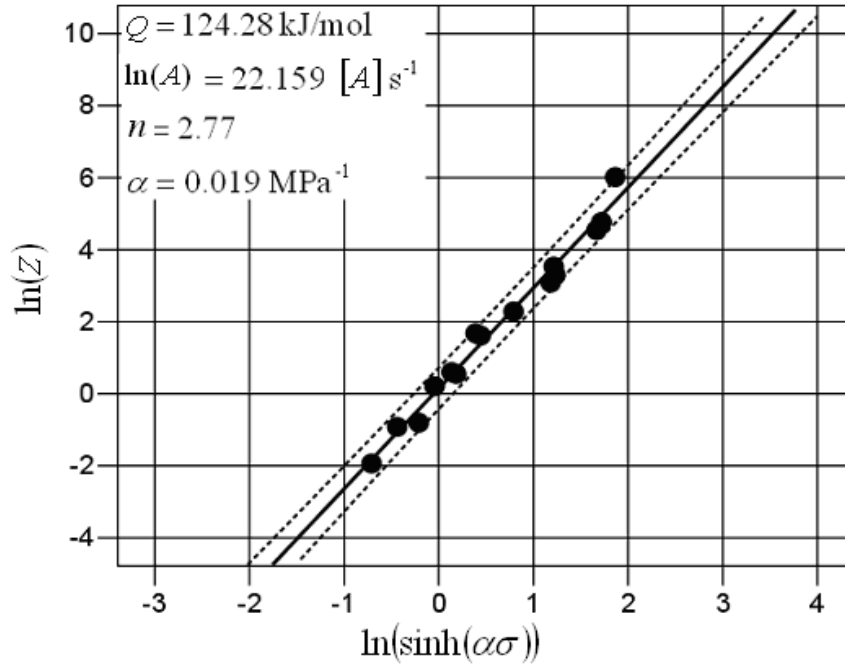


Figure 5. Relationship between the Zener-Hollomon parameter and the stress at $\varepsilon=0.4$ for the AZ31 alloy. The continuous line is the fit obtained with the Garofalo parameters, given in the figure, obtained by the RCR model and the dashed lines are the upper and lower limits for the confidence intervals attributed to the predicted results.

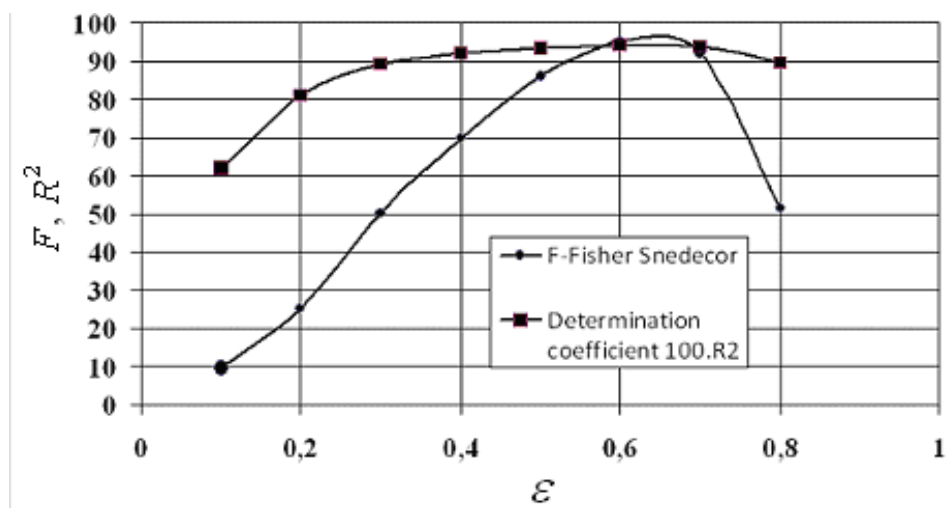


Figure 6. Strain dependence of statistical parameters controlling the model quality.

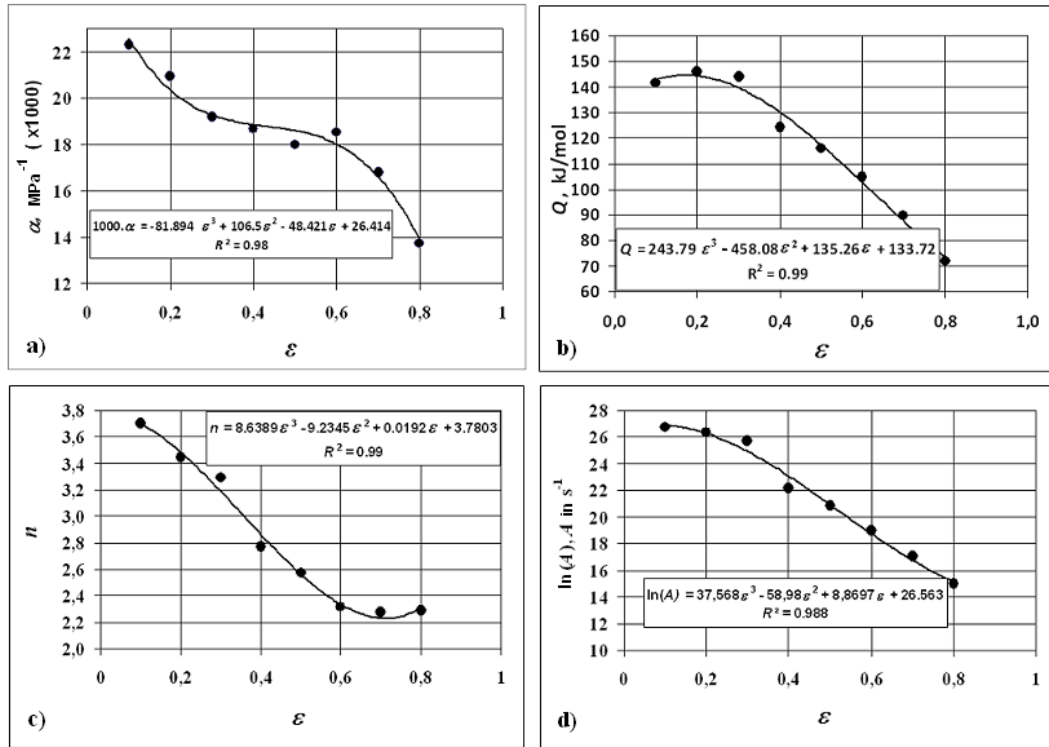


Figure 7. Representation of the four Garofalo parameters as a function of strain for the AZ31 alloy. The continuous line in each subplot corresponds to the best fit. The equations used for the fit are given in the figure legends.

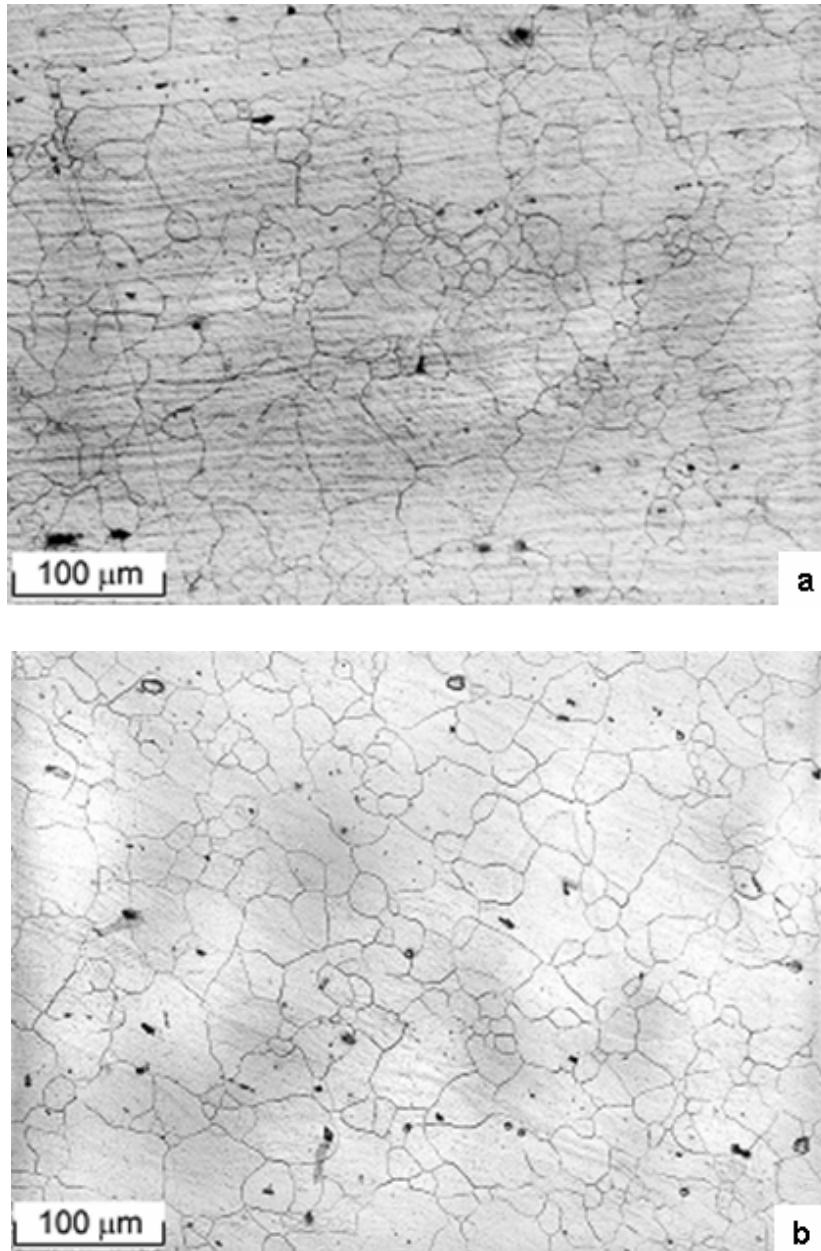


Figure 8. Micrographs of AZ31 alloy obtained (a) before torsion testing and (b) after torsion testing at 419°C/2 s⁻¹.

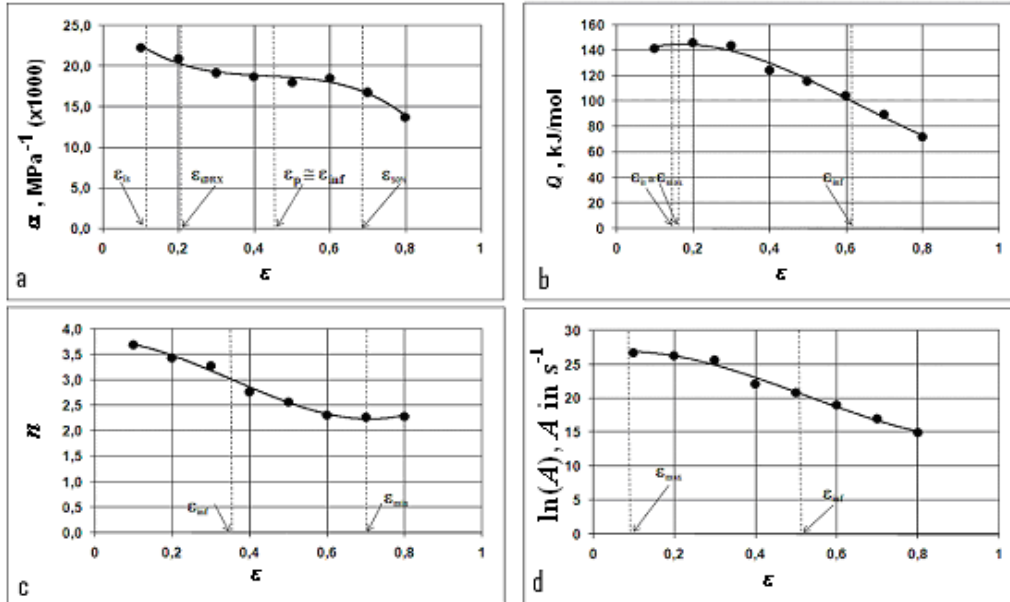


Figure 9. Variation of parameters of Garofalo equation with strain. The principal strain values that characterize the microstructural evolution of the AZ31 alloy are indicated. Tables 4 and 5 define the strains given in the graphs.

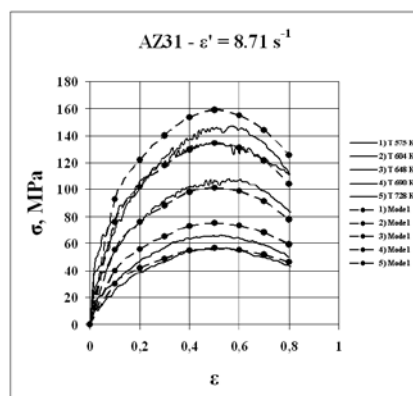
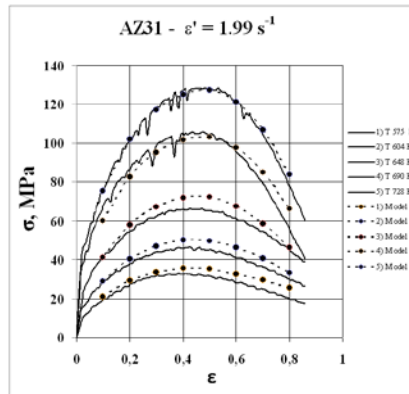
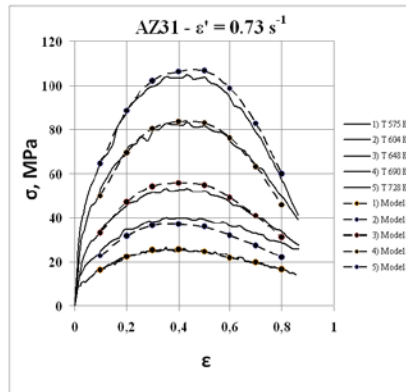


Figure 10. Strain-stress curves from experimental data (continuous lines) and from model predictions (dashed lines) at various temperatures at (a) 0.73 s^{-1} , (b) 1.99 s^{-1} and (c) 8.71 s^{-1} .